ROYAL SOCIETY
OF CHEMISTRY

PAPER

Check for updates

Discovery of new pyridine heterocyclic hybrids; design, synthesis, dynamic simulations, and *in vitro* and *in vivo* breast cancer biological assays†

Menna M. Abdelshaheed,[a] Hussein I. El Subbagh,[b] Mohamed A. Tantawy,[cdg]
Reem T. Attia,[e] Khairia M. Youssef[f] and Iten M. Fawzy [ID] *[f]

Pyridine is a nitrogen bearing heterocyclic scaffold that shows a wide range of biological activities. The pyridine nucleus has become an interesting target for medicinal chemistry researchers worldwide. Several pyridine derivatives exhibited good anticancer effects against diverse cell lines. Therefore, to explore new anticancer pyridine entities, novel pyridine derivatives were designed and synthesized and evaluated for their anticancer abilities *in vitro* and *in vivo*. All of the target compounds were evaluated against three different human cancer cell lines (Huh-7, A549 and MCF-7) *via* MTT assay. Most of the compounds exhibited significant cytotoxic activities. Compounds **3a**, **3b**, **5a** and **5b** showed superior antiproliferative activities to Taxol. Where, compound **3b** showed IC_{50} values of 6.54, 15.54 and 6.13 μM compared to Taxol (6.68, 38.05, 12.32 μM) against Huh-7, A549 and MCF-7, respectively. Also, tubulin polymerization assay was carried out. The most potent compounds **3a**, **3b**, **5a** and **5b** could significantly inhibit tubulin polymerization with IC_{50} values of 15.6, 4.03, 6.06 and 12.61 μM, respectively. Compound **3b** exhibited the highest tubulin polymerization inhibitory effect with an IC_{50} value of 4.03 μM compared to combretastatin (A-4) (1.64 μM). Molecular modeling studies of the designed compounds confirmed that most of the compounds made the essential binding interactions compared to the reference compound which assisted in the prediction of the structure requirements for the detected anticancer activity. Finally, *in vivo* studies showed that compound **3b** could significantly inhibit breast cancer.

1. Introduction

Cancer, uncontrolled cell growth, is a fatal disease. It is also one of the top leading causes of death worldwide. Cancer deaths are predicted to increase from 7.6 million in 2008 to 13 million in 2030.[1,2] Despite improved diagnostic techniques, cancer still affects millions of patients worldwide.[3] Although chemotherapy is the most common treatment of cancer, many chemotherapeutic agents cause severe side effects due to their cytotoxic and mutagenic effects on healthy cells. Notably, pyridine has been used as a key pharmacophore in drug design with an improved safety profile and less toxicity to non-tumorigenic cells. Several pyridine derivatives were reported to inhibit enzymes, receptors, and other targets to control and cure cancer. Therefore, researchers are currently focusing on the development of pyridine-based novel derivatives for cancer treatment.[4–6]

Literature survey showed that different fused rings bearing pyridine moiety exhibited anticancer activity such as pyrano[3,2-*c*] pyridine, pyrido[4,3-*d*]-pyrimidine and pyrazolo[4,3-*c*] pyridine derivatives[13] (Fig. 1). These reported fused rings were proved to be potent and selective antitumor agents.

Dynamic microtubules play an essential role in variable cellular processes such as intracellular trafficking, cell migration, cell skeleton development and cell division.[14–16]

Tubulin polymerization inhibitors are increasingly being investigated as anti-cancer drugs. Whereas microtubule targeting agents (MTAs) can interfere with microtubule dynamics and arrest cancer cells in the G2/M phase, therefore cancer cells undergo apoptosis.[17–19]

Compounds that bind to the colchicine site (Fig. 2) have been widely studied to find new agents that can deal with the

[a]Department of Pharmaceutical Chemistry, Faculty of Pharmacy, Horus University in Egypt, New Damietta, Egypt

[b]Department of Medicinal Chemistry, Faculty of Pharmacy, Mansoura University, P.O. Box 35516, Mansoura, Egypt

[c]Hormones Department, Medical Research and Clinical Studies Institute, National Research Centre, Dokki, Giza, Egypt

[d]Stem Cells Lab, Center of Excellence for Advanced Sciences, National Research Centre, Dokki, Cairo, Egypt

[e]Department of Pharmacology and Toxicology and Biochemistry, Faculty of Pharmacy, Future University in Egypt, 11835, Cairo, Egypt

[f]Department of Pharmaceutical Chemistry, Faculty of Pharmacy, Future University in Egypt, 11835, Cairo, Egypt. E-mail: iten.mamdouh@fue.edu.eg; Tel: +201006064161

[g]Department of Orthopaedics and Rehabilitation, CORTS, Penn State University, College of Medicine, 500 University Drive, Hershey, PA 17033-0850, USA

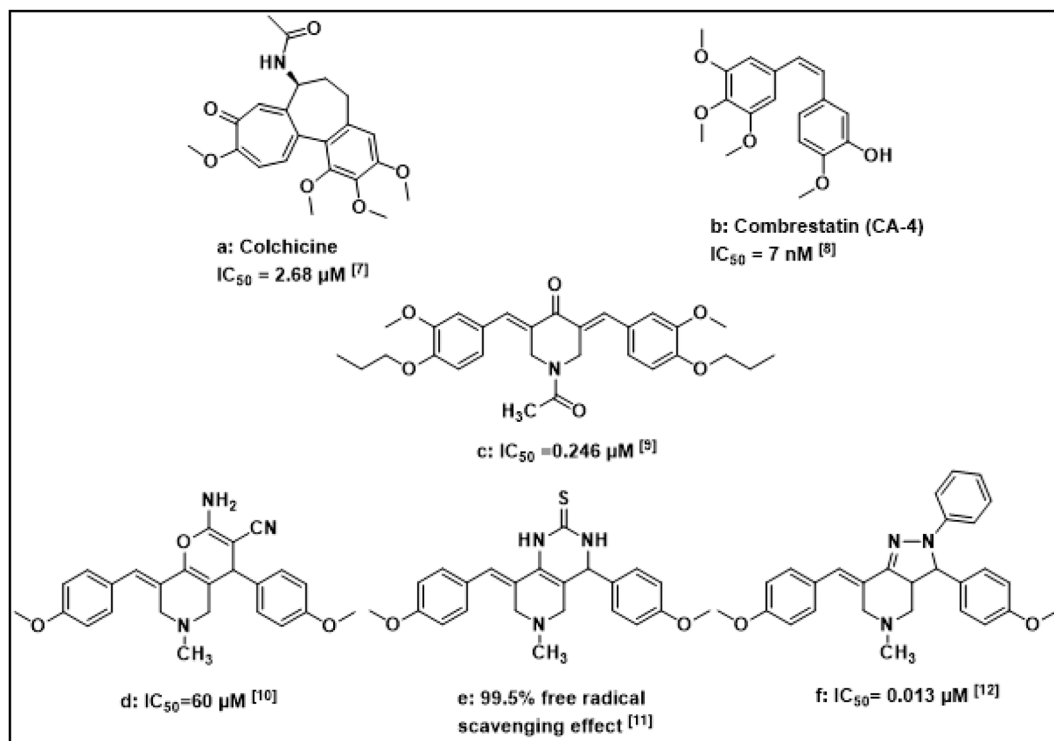† Electronic supplementary information (ESI) available. See DOI: https://doi.org/10.1039/d3ra02875e

Fig. 1 Reported antitumor agents with fused rings–pyridine bearing nucleus.[7–12]

limitations of existing tubulin-targeted drugs.[20] Disruption of tubulin polymerization is an old anticancer target, however, this target is still one of the hit targets for discovery of anticancer agents. Several new anticancer drugs have been discovered *via* the microtubule/tubulin interaction-based drug design. Taxol has been a popular representative for tubulin-interactive targeting drugs which was used for many years as anticancer. Meanwhile, there have been emerging scaffolds of tubulin-interactive natural products as combretastatin A-4, epothilones A and B, halichondrin B, thiazole alkaloid, phenylahistin, diketopiperazine and dolastatin 10 peptide.[21]
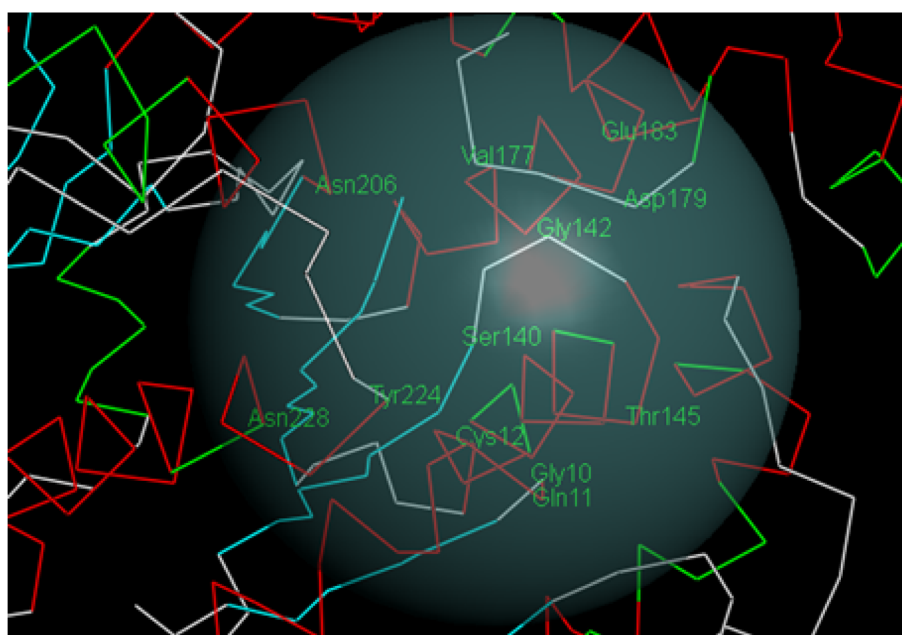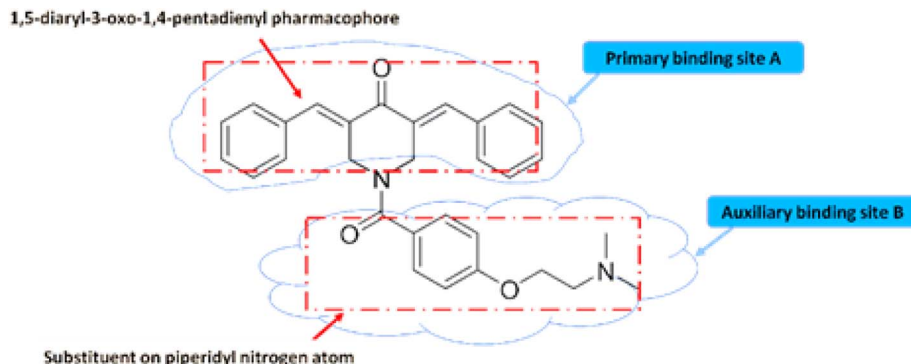

Fig. 2 Colchicine binding site.

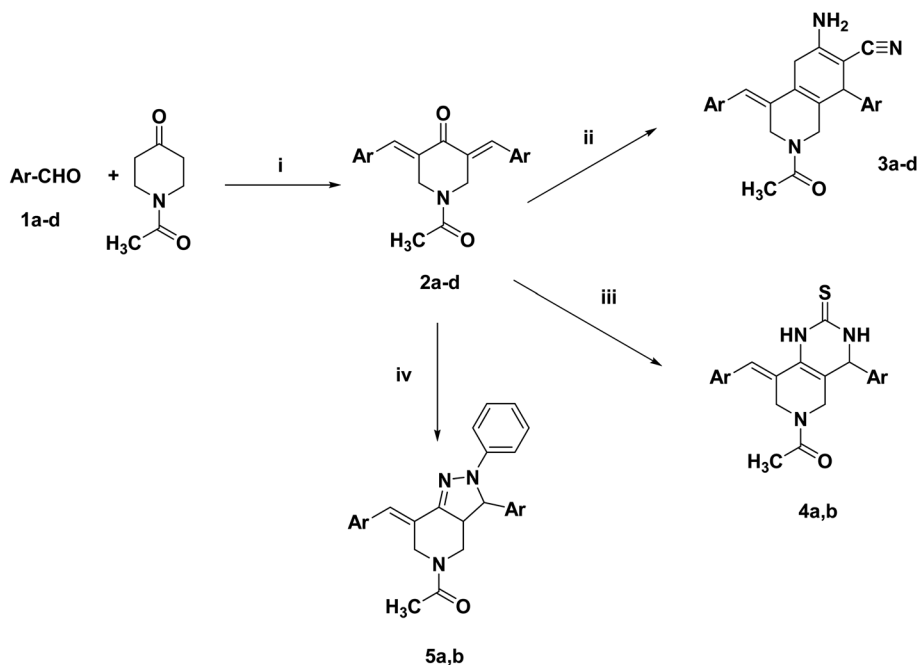**Fig. 3** Essential structural features of piperidone analogues.

Combretastatin A-4 (**CA-4**) (Fig. 1) is a strong antitumor agent which was isolated from *Combretum caffrum* family. **CA-4** acts by inhibiting polymerisation of tubulin at colchicine binding site. Trimethoxyphenyl (TMP) moiety in **CA-4** was found to be essential for activity as the methoxy group is responsible for the critical hydrogen bond with Cys 12.[22–24] Therefore, methoxy groups were preserved in most anticancer agents targeting colchicine binding site.

In this study new pyridine heterocyclic hybrids were developed using pyran, pyrimidine and pyrazole rings. The synthesized hybrids were evaluated for their antiproliferative activity against three types of cancer cell lines: hepatocyte derived carcinoma, lung, and breast cancer cell lines. Meanwhile, the compounds were tested for their depolymerization ability towards tubulin. This was deeply illustrated *via* molecular docking and dynamic simulation studies. The most active compound was selected for *in vivo* activity investigation against breast cancer.

2. Experimental

The ^{1}H NMR spectra were recorded on JEOL 500 MHz spectrometer at the faculty of science, Mansoura University whereas ^{13}C NMR spectra were recorded on JEOL 125 MHz spectrometer in which TMS was used as an internal standard and chemical shifts were expressed as ppm and coupling constants (*J*) were given in Hz. Chemical shifts are given on the delta (*d*) scale in parts per million (ppm). Mass spectrometer (Hewlett Packard

i: Conc. HCl, 2h, r.t., ii: malononitrile, butanol, 5h, reflux, yield: 82-70%, iii: thiourea, Na metal, butanol, 10h, reflux, yield: 80-78%, iv: phenylhydrazine, Na metal, ethanol, 10h, reflux, yield: 72-74%

Scheme 1 Synthetic scheme of pyridine heterocyclic hybrids target compounds.

Table 1 IC$_{50}$ of new target compounds tested on three different cancer cell lines[a]

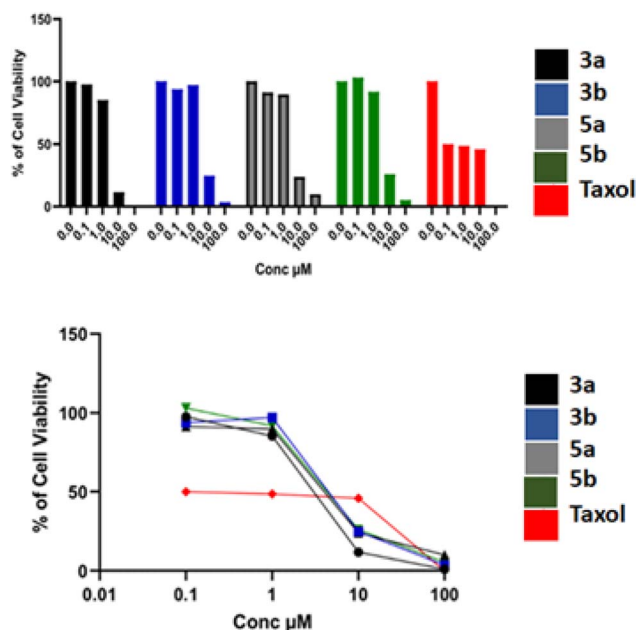| Compounds	Human hepatoma (Huh-7) IC$_{50}$ in μM	Lung cell cancer adenocarcinoma (A549) IC$_{50}$ in μM	Michigan cancer foundation-7 breast cancer (MCF-7) IC$_{50}$ in μM
3a	3.88	31.59	8.87
3b	6.54	15.54	6.13
3c	17.70	61.25	6.38
3d	20.72	ND	ND
4a	2.48	46.90	8.01
4b	7.27	42.34	15.97
5a	5.47	20.26	5.27
5b	2.23	15.15	9.04
Taxol	6.68	38.05	12.32

[a] ND = not defined.

Fig. 4 Toxicity effect of selected compounds on (MDCK) cells as non-cancerous cell line.

5988) was utilised to record on spectrometer at Regional Centre for Mycology and Biotechnology, Al-Azhar University. Elemental analyses (%C, H, N, S) were also performed using (Thermo Scientific c Flash 2000 elemental analyser) at the Regional Center for Mycology and Biotechnology, Al-Azhar University and the results were in accordance with the proposed structures. Melting points were determined using capillary tubes with a Stuart SMP30 apparatus and are uncorrected. Progression of the reactions was monitored using TLC Merck Kieselgel 60 F254 aluminum packed plates.

2.1. General procedure for synthesis of (2a–d) intermediates

The intermediate compounds **2a–d** were prepared with a procedure similar to a condensation reaction obtained from literature where (0.02 mol) of the appropriate aldehyde was added and condensed with (0.01 mol/1.41 ml) of *N*-acetyl-4-piperidone and then heated in a water bath at 25–30 °C until

a clear solution was gained, then 4 ml of concentrated HCl was added dropwise while stirring for 5 min. The reaction mixture was eventually stirred at room temperature for 2 h. The mixture was left standing for 2 days, then it was treated with cold AcOH/water (1 : 1) and filtered. The solid obtained was then dried well and recrystallized from methanol/ethanol. The obtained intermediates were reported[25] & their characterization coincided with those in literature.

2.2. General procedure for synthesis of (3a–d) target compounds

A mixture of diarylidene compounds **2a–d** (0.01 mol) and malononitrile (0.7 g, 0.01 mol) in butanol (50 ml) was heated under reflux for 5 h. Evaporation of the solvent yielded the target compounds which were then washed, filtered off, dried, and recrystallized from ethanol.[26]

2.2.1 (*E*)-6-Acetyl-2-amino-3-cyano-8-(4-hydroxy-3-methoxybenzylidene)-4-(4-hydroxy-3-methoxyphenyl)-5,6,7,8-tetrahydro-4*H*-pyrano[3,2-*c*]pyridine: (3a). The titled compound was crystallised from ethanol and separated as yellow powder with: yield%: 76%, melting point: 205–207 °C. FT-IR (v_{max}, cm^{-1}): 3550–3000 broad band of (O–H), 3400 & 3300 two bands of (N–H), 3010 (Ar C–H), 2250 (C≡N), 1680 (alkenic C=C–) and 1715 (C=O of amide). Ms: *m/z*%: 475.50 [M+] (45.73%). ^{1}H-NMR (400 MHz, DMSO-d$_6$) δ 9.70 (s, 2H, OH, D$_2$O exchangeable), 7.61 (s, 1H, CH=C), 7.58 (dd, *J* = 7.5, 8.9 Hz, 2H, ArH), 7.11–7.09 (dd, *J* = 8 Hz, 2H, ArH), 7.00 (s, 1H, ArH), 6.87 (s, 2H, NH$_2$ D$_2$O exchangeable), 6.86 (s, 1H, ArH), 6.85 (s, 1H, C4–H), 4.77 (s, 2H, CH$_2$–N), 4.75 (s, 2H, CH$_2$–N), 3.80 (s, 3H, CH$_3$–O), 3.78 (s, 3H, CH$_3$–O), 1.87 (s, 3H, CH$_3$). ^{13}C-NMR (300 MHz, DMSO-d$_6$): δ 185.76(C=O), 168.75 (C–NH$_2$), 148.60 (ArC), 148.58 (C=C), 136.71, 136.50, 129.97, 129.79, 126.02, 125.78, 124.47 (ArC), 124.42 (C=C), 115.84 (C=C), 115.80 (C=C), 115.09 (CN), 115.01 (C–CN), 55.72 (O–CH$_3$) 47.11 (C4), 42.43 (CH$_2$NCH$_2$), 20.93 (CH$_3$). Anal. calcd. for C$_{26}$H$_{25}$N$_3$O$_6$ (475.50): C, 65.68; H, 5.30; N, 8.84, found: C, 65.82; H, 5.41; N, 9.07.

2.2.2. (*E*)-6-Acetyl-2-amino-3-cyano-4-(3-ethoxy-4-hydroxyphenyl)-8-(3-ethoxy-4-hydroxy-benzylidene)-5,6,7,8-tetrahydro-4*H*-pyrano[3,2-*c*]pyridine: (3b). The titled compound was crystallised from ethanol and separated as yellowish green powder with: yield%: 82%, melting point:200–202 °C. FT-IR
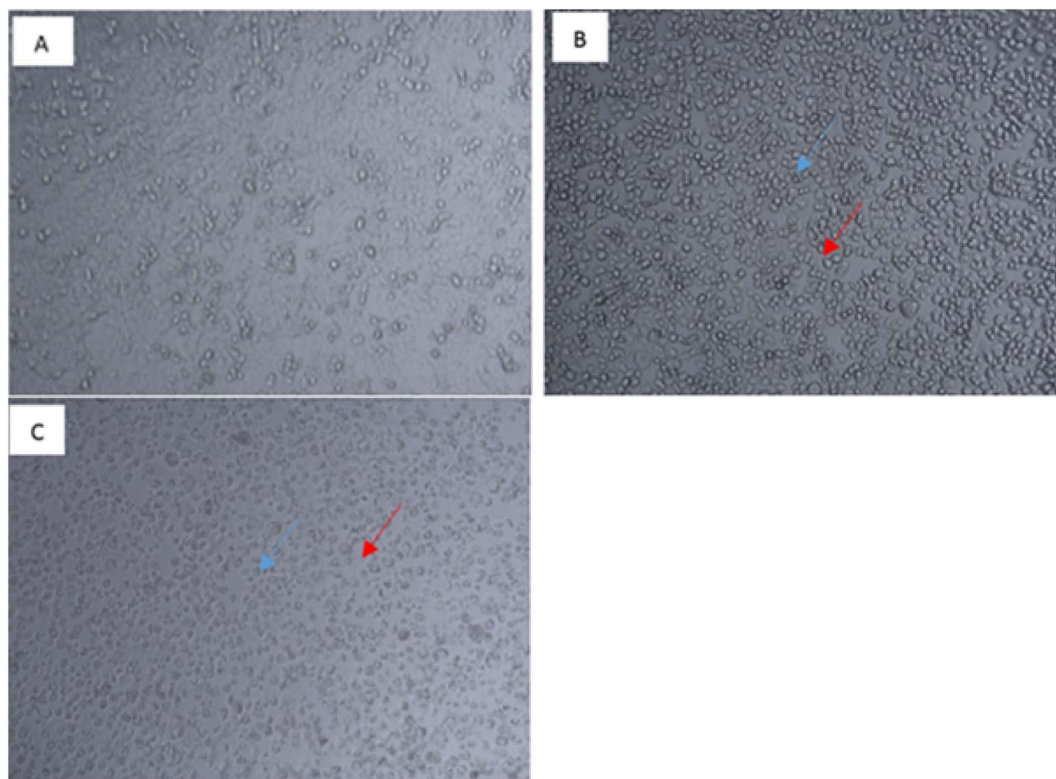
Fig. 5 Morphological assessment for (A549) cells: (A) control untreated cells, (B) (A549) treated cells with 100 µM of compound "**3b**" at 48 h (C) (A549) treated cells with 100 µM of Taxol at 48 h.

Table 2 Results of *in vitro* tubulin inhibition assay

Compound	Inhibition (%)	IC_{50} in µg ml^{-1}
3a	79	15.6
3b	81	4.03
5a	76	6.06
5b	70	12.61
CA-4	86	1.64

(ν_{max}, cm^{-1}): 3550–3000 broad band of (O–H), 3300 (N–H), 3010 (Ar C–H), 2250 (C≡N),1680 (alkenic C=C–) and 1715 (C=O of amide). Ms: $m/z\%$: 504.21 [M+] (30.3%). ^{1}H-NMR (400 MHz, DMSO-d$_6$) δ 9.61 (s, 2H, OH, D$_2$O exchangeable), 7.56 (s, 1H, CH=C), 7.07 (dd, J = 7.9, 8.5 Hz, 2H, ArH), 6.98 (s, 2H, NH$_2$ D$_2$O exchangeable), 6.99 (s, 1H, ArH), 6.95 (s, 1H, ArH), 6.87 (dd, J = 8 Hz, 2H, ArH), 4.75 (s, 2H, CH$_2$–N), 4.74 (s, 2H, CH$_2$–N), 4.07 (s, 1H, C4–H), 4.01–4.06 (q, J = 8 Hz, 4H, O–CH$_2$–CH$_3$), 1.87 (s, 3H, CH$_3$), 1.31 (t, J = 7.5 Hz, 6H, CH$_3$–CH$_2$–O). ^{13}C-NMR (300 MHz, DMSO-d$_6$): δ 185.69 (C=O), 168.65 (C–NH$_2$), 148.82 (ArC), 146.76 (C=C), 146.73, 136.66, 136.46, 129.87, 129.71, 125.96 (ArC), 125.72 (C=C), 124.48 (C=C), 116.21 (C=C), 116.12(CN), 115.87 (C–CN), 63.92 (CH$_2$–CH$_3$), 63.86 (CH$_2$–CH$_3$) 47.05 (C4), 42.37 (CH$_2$–N–CH$_2$), 20.90 (CH$_3$) 14.71 (CH$_3$–CH$_2$). Anal. calcd. for C$_{28}$H$_{29}$N$_3$O$_6$ (503.56): C, 66.79; H, 5.81; N, 8.34, found: C, 66.82; H, 5.77; N, 8.29.

2.2.3. (*E*)-6-Acetyl-2-amino-3-cyano-8-(4-chlorobenzylidene)-4-(4-chlorophenyl)-5,6,7,8-tetrahydro-4*H*-pyrano [3,2-*c*]pyridine: (3c). The titled compound was crystallised from ethanol and separated as yellow powder with: yield%: 76%, melting point: 198–200 °C. FT-IR (ν_{max}, cm^{-1}): 3400 & 3300 two bands of (N–H), 3010 (Ar C–H), 2250 (C≡N), 1680 (alkenic C=C–) and 1650 (C=O of amide), 850 (C–Cl). Ms: $m/z\%$: 453.08 [M+] (63.9%). ^{1}H-NMR (400 MHz, DMSO-d$_6$) δ 7.63 (s, 1H, CH=C), 7.58 (dd, J = 8, 7.7 Hz, 2H, ArH), 7.57 (dd, J = 7.5, 8.2 Hz, 2H, ArH), 7.55 (dd, J = 8, 7.4 Hz, 2H, ArH), 7.54 (dd, J = 8, 7.6 Hz, 2H, ArH), 7.53 (s, 2H, NH$_2$ D$_2$O exchangeable), 7.52 (s, 1H, C4–H) 4.75 (s, 2H, CH$_2$–N), 4.74 (s, 2H, CH$_2$–N), 1.84 (s, 3H, CH$_3$). ^{13}C-NMR (300 MHz, DMSO-d$_6$): δ 185.3(C=O), 161.4 (C–NH$_2$), 148.58 (ArC), 142.9 (C=C),142.4, 136.8, 134.4, 130.8, 129.1, 129.0, 128.7 (ArC), 124.42 (C=C), 115.84 (C=C), 115.80 (C=C), 115.09 (CN), 115.01 (C–CN), 55.72 (CH$_2$–CH$_3$), 47.11 (C4), 42.43 (CH$_2$–N–CH$_2$), 20.93 (CH$_3$). Anal. calcd. for C$_{24}$H$_{19}$Cl$_2$N$_3$O$_2$ (452.34): C, 63.73; H, 4.23; Cl, 15.67; N, 9.29, found: C, 63.53; H, 4.25; Cl, 15.70; N, 9.20.

2.2.4. (*E*)-6-Acetyl-2-amino-3-cyano-8-((*E*)-3-phenyl-allylidene)-4-((*E*)-styryl)-5,6,7,8-tetrahydro-4*H*-pyrano[3,2-*c*]pyridine: (3d). The titled compound was separated as green powder with yield%: 70%, melting point: 168–170 °C. FT-IR (ν_{max},cm^{-1}): 3400 and 3300 two bands of (N–H), 3010 (Ar C–H), 2250 (C≡N), 1680 (alkenic C=C–) and 1715 (C=O of amide). Ms: $m/z\%$: 436.20 [M+] (30.3%). ^{1}H-NMR (400 MHz, DMSO-d$_6$) δ 7.68 (dd, J = 7.4, 8 Hz, 2H, ArH), 7.41 (dd, J = 7.5, 8.4 Hz, 2H, ArH),
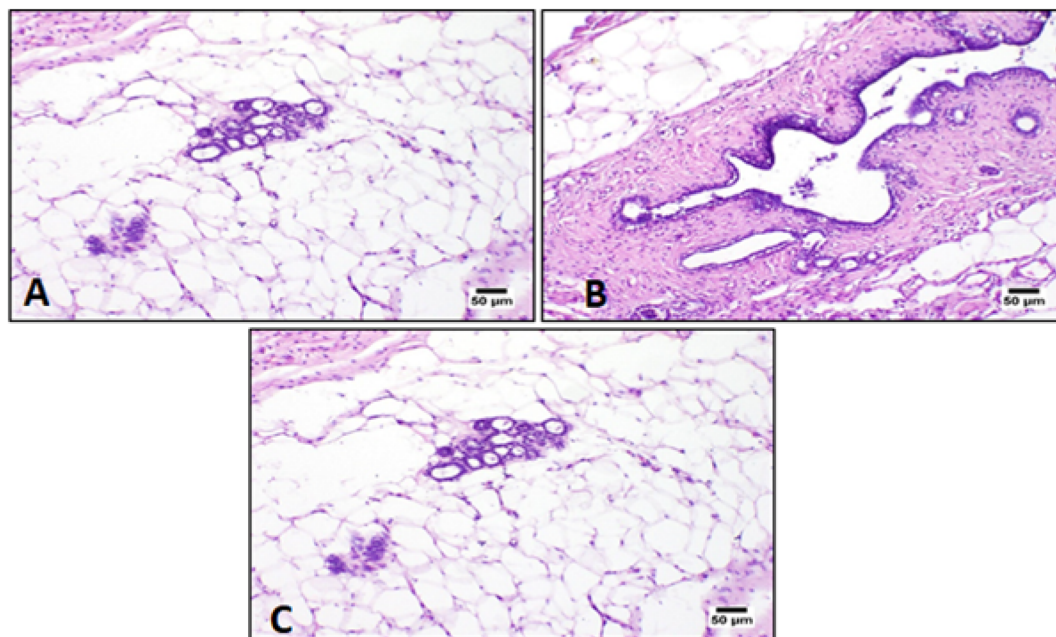
Fig. 6 Photomicrograph of mammary gland from control group showing normal (A) histological structure, with (B) a major duct lined with cuboidal epithelium and (C) a normal duct and few acini embedded in adipose tissue (H&E).

7.37 (t, J = 8 Hz, 4H, ArH), 7.34 (t, J = 7.4 Hz, 2H, ArH), 7.30 (t, J = 7.6 Hz, CH=CH), 7.28 (d, J = 8 Hz, 1H, CH=CH), 7.24 (d, J = 8 Hz, 1H, CH=CH), 7.22 (s, 2H, NH$_2$, D$_2$O exchangeable), 7.21 (d, J = 8 Hz, 1H, CH=CH), 7.18 (t, J = 7.5 Hz, 1H, CH=CH), 7.15 (d, J = 7.5 Hz, 1H, C4–H), 4.72 (s, 2H, CH$_2$–N), 4.71 (s, 2H, CH$_2$–N), 2.10 (s, 3H, CH$_3$). ^{13}C-NMR (300 MHz, DMSO-d$_6$): δ 185.23 (C=O), 168.79 (C–NH$_2$), 142.60, 142.49 (ArC), 136.27 (C=C), 136.17 (ArC) 135.70 (C=C), 135.29, 131.78, 131.44 (ArC), 129.34, 128.88, 128.53 (C=C), 127.70, 127.31 (ArC), 123.04 (CN), 60.37 (C–CN), 45.62 (1C, C4) 41.58 (1C, CH$_2$–N), 34.70 (CH$_2$–N), 21.21 (1C, CH$_3$). Anal. calcd. for C$_{28}$H$_{25}$N$_3$O$_2$ (435.53): C, 77.22; H, 5.79; N, 9.65 found: C, 67.05; H, 5.97; N, 8.50.

2.3. General procedure for synthesis of (4a, b) target compounds

To a mixture of the diarylidene compound **2a/b** (0.01 mol) and thiourea (0.8 g, 0.01 mol), sodium butoxide was added (Na metal (0.5 g) in butanol (50 ml)) and heated under reflux for 10 h.[27] The solvent used was evaporated *in vacuo*, water (20 ml) was then added, and the mixture was neutralized to pH 6. The separated solid was then filtered, washed, dried, and recrystallized from ethanol.

2.3.1. (*E*)-6-Acetyl-8-(4-hydroxy-3-methoxybenzylidene)-4-(4-hydroxy-3-methoxyphenyl)-1,3,4,5,7,8-hexahydro-2*H*-pyrido[4,3-*d*]pyrimidin-2-thione: (4a). The titled compound was crystallised from methanol and separated as yellow powder with: yield%: 80%, melting point: 188–190 °C. FT-IR (ν_{max}, cm^{-1}): 3550–3000 broad band of (O–H), 3300 (N–H), 3010 (Ar C–H), 1680 (alkenic C=C–) and 1715 (C=O of amide). Ms: m/z: 468.15 [M+] (26.0%). ^{1}H-NMR (400 MHz, DMSO-d$_6$) δ 9.70 (s, 2H, OH, D$_2$O exchangeable), 7.61 (s, 1H, NH–CH, D$_2$O exchangeable), 7.58 (s, 1H, NH, D$_2$O exchangeable), 7.10 (s, 1H, CH=C), 7.08 (s,

1H, ArH), 7.01 (s, 1H, ArH), 6.99–6.97 (dd, J = 8, 7.1 Hz, 2H, ArH), 6.87–6.85 (dd, J = 8, 7.2 Hz, 2H, ArH), 4.77 (d, 1H, C4–H), 4.77 (s, 2H, CH$_2$-N), 4.75 (s, 2H, CH$_2$-N), 3.80 (s, 3H, CH$_3$–O), 3.78 (s, 3H, CH$_3$–O), 1.87 (s, 3H, CH$_3$). ^{13}C-NMR (300 MHz, DMSO-d$_6$) δ 184.61 (C=S), 169.04 (C=O), 157.14, 149.75, 149.58 (ArC), 137.60 (C–NH), 126.99, 126.87, 126.18 (ArC), 121.66 (C=C), 121.01, 117.70, 117.52, 114.82, 114.69 (ArC), 55.76 (CH$_3$–O), 55.71 (CH–NH), 47.72 (CH$_2$–N), 43.09 (1C, CH$_2$–N), 21.42 (1C, CH$_3$). Anal. calcd for C$_{24}$H$_{25}$N$_3$O$_5$S (467.54): C, 61.66; H, 5.39; N, 8.99; S, 6.86 found: C, 63.24; H, 6.08; N, 8.70; S, 6.53.

2.3.2. (*E*)-6-Acetyl-8-(3-ethoxy-4-hydroxybenzylidene)-4-(3-ethoxy-4-hydroxyphenyl)-1,3,4,5,7,8-hexahydro-2*H*-pyrido[4,3-*d*]pyrimidin-2-thione: (4b). The titled compound was separated from methanol as greenish yellow powder with: yield%: 78%, melting point: 208–210 °C. FT-IR (ν_{max}, cm^{-1}): 3550–3000 broad band of (O–H), 3300 (N–H), 3010 (Ar C–H), 1680 (alkenic C=C–) and 1715 (C=O of amide). Ms: m/z: 495.71 [M+] (34.0%). ^{1}H-NMR (400 MHz, DMSO-d$_6$): δ 7.50 (s, 1H, OH, D$_2$O exchangeable), 7.49 (s, 1H, OH, D$_2$O exchangeable), 6.89 (s, 1H, NH–CH, D$_2$O exchangeable), 6.86 (s, 1H, NH, D$_2$O exchangeable), 6.85 (s, 1H, CH=C), 6.57 (s, 1H, ArH), 6.55 (s, 1H, ArH), 6.53 (dd, J = 8, 7.2 Hz, 2H, ArH), 6.51 (dd, J = 8.2, 8.7 Hz, 2H, ArH) 4.73 (s, 1H, C4–H), 4.70 (s, 2H, CH$_2$–N), 4.67 (s, 2H, CH$_2$–N), 3.99–3.97 (dd, J = 7.0, 7.2 Hz, 4H, CH$_2$–CH$_3$),1.88 (s, 3H, CH$_3$), 1.28 (t, J = 6.9 Hz, 6H, CH$_3$–CH$_2$). ^{13}C-NMR (300 MHz, DMSO-d$_6$): δ 184.61 (1C, C=S), 169.04 (1C, C=O), 157.14,149.75, 149.58 (ArC), 137.60 (C–NH), 126.99 126.87 126.18 (ArC), 121.66 (1C, C=C), 121.01, 117.70, 117.52, 114.82, 114.69 (ArC), 55.76 (CH$_3$–O), 55.71 (CH–NH), 47.72 (CH$_2$–N), 43.09 (CH$_2$–N), 21.42 (1C, CH$_3$). Anal. calcd. for C$_{26}$H$_{29}$N$_3$O$_5$S (495.59): C, 63.01; H, 5.90; N, 8.48; S, 6.47 found: C, 73.25; H, 6.08; N, 9.16; S, 7.61.
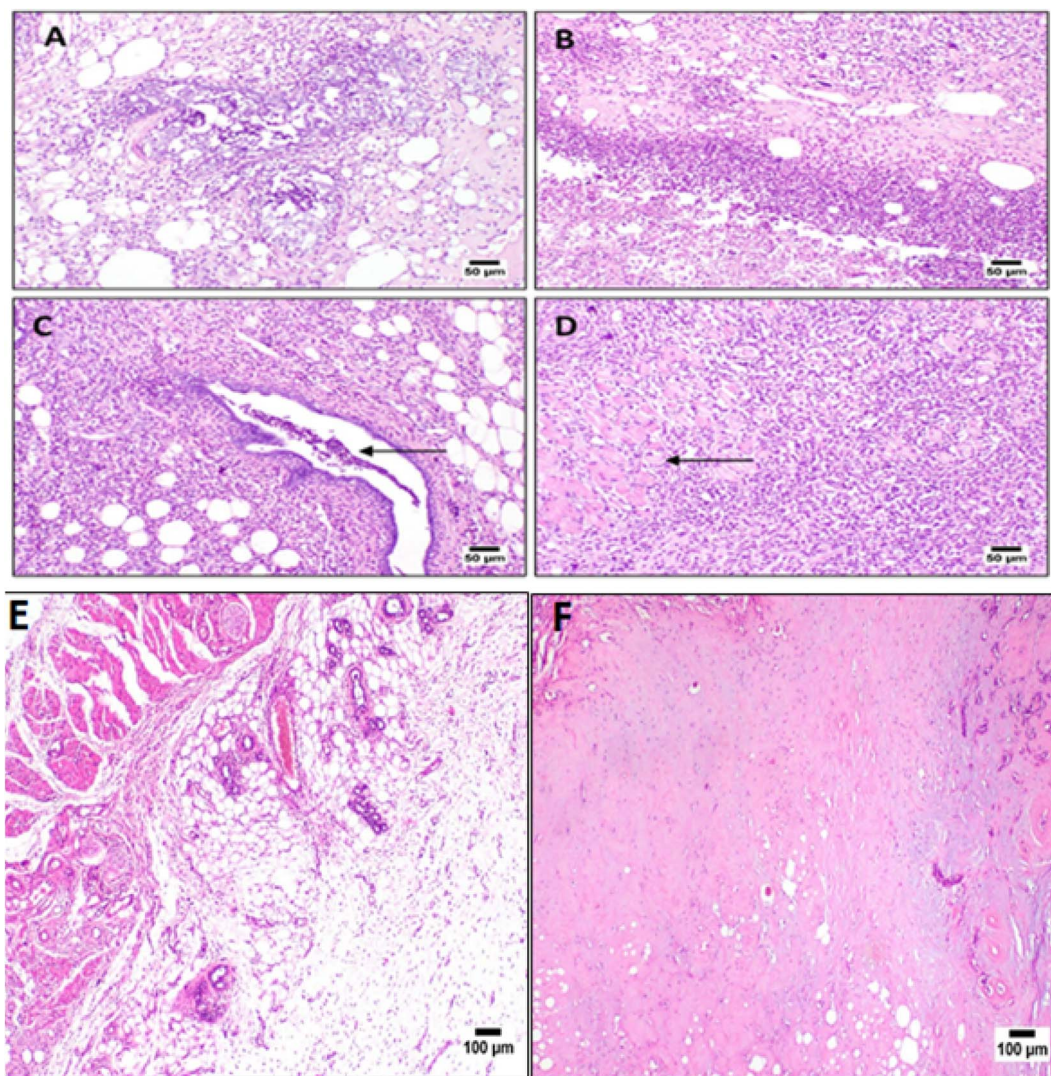
Fig. 7 Photomicrograph of mammary gland from breast cancer (BC) group showing (A) invasion of the neoplastic cells admixed with mono-nuclear cells and necrotic debris. (B) Heavy mononuclear inflammatory cells infiltrating the dermal layer. (C) Invasion of the neoplastic cells into the adjacent tissue with numerous mononuclear cells infiltration (arrow). (D) Photomicrograph of mammary gland from (BC) group showing heavy mononuclear inflammatory cells infiltrating the adjacent muscle bundles. (E) Taxol treatment group, showing fewer mononuclear inflammatory cells infiltration with less congested blood vessels (H&E). (F) Photomicrograph of mammary gland from **3b** treated group showing minimal inflammatory reactions (H&E).

2.4. General procedure for synthesis of 5a, b target compounds

In a flask containing phenyl hydrazine (4.3 g, 0.04 mol) and diarylidene compound **2a/b**, (0.01 mol), sodium butoxide prepared (Na metal (0.5 g) in ethanol (50 ml)) was added and subjected to reflux for 10 h.[28] The solvent was then removed under reduced pressure and the remaining residue was chromatographed on silica gel ($CHCl_3$) to furnish compounds **5a, b**.

2.4.1. (E)-5-Acetyl-7-(4-hydroxy-3-methoxybenzylidene)-3-(4-hydroxy-3-methoxyphenyl)-2-phenyl-2,3,3a,4,6,7-hexahydro-5H-pyrazolo[4,3-c]pyridine (5a).
The titled compound was separated as yellow powder with: yield%: 72%, melting point: 190–192 °C. FT-IR (ν_{max}, cm^{-1}): 3550–3000 broad band of (O–H), 3010 (Ar C–H),1680 (alkenic C=C–) and 1715 (C=O of amide). Ms: m/z%: 501.22 [M+] (2.0%). ^{1}H-NMR (400 MHz, DMSO-d$_6$):

δ 9.69 (s, 2H, OH, D$_2$O exchangeable), 7.11 (s, 1H, CH=C), 7.09 (dd, J = 7.2, 8 Hz, 2H, ArH), 7.01 (t, J = 7.8 Hz, 1H, ArH), 6.99–6.99 (t, J = 8 Hz, 2H, ArH), 6.97 (dd, J = 8, 7.9 Hz, 4H, ArH), 6.88 (s, 2H, ArH), 6.85 (d, 1H, C3–H), 4.77 (s, 2H, CH$_2$–N), 4.76 (d, 2H, CH$_2$–N), 3.79 (s, 6H, CH$_3$–O), 3.77 (q, J = 7.4 Hz, 1H, C3a–H), 1.88 (s, 3H, CH$_3$). ^{13}C-NMR (300 MHz, DMSO-d$_6$): δ 186.19 (C=O), 169.15 (C=N), 137.11, 136.91 (ArC), 130.41 (C=C), 130.23 (C=C), 126.45, 126.21, 124.90, 124.84, 116.27, 115.55 (ArC), 115.47 (C=C), 56.17 (1C, C3), 47.53 (1C, C3a), 42.87 (CH$_2$–N–CH$_2$), 21.36 (CH$_3$). Anal. calcd. for C$_{29}$H$_{29}$N$_3$O$_5$ (499.57): C, 69.72; H, 5.85; N, 8.41, found: C, 69.72; H, 5.85; N, 8.41.

2.4.2. (E)-5-Acetyl-7-(3-ethoxy-4-hydroxybenzylidene)-3-(3-ethoxy-4-hydroxyphenyl)-2-phenyl-2,3,3a,4,6,7-hexahydro-5H-pyrazolo[4,3-c]pyridine (5b).
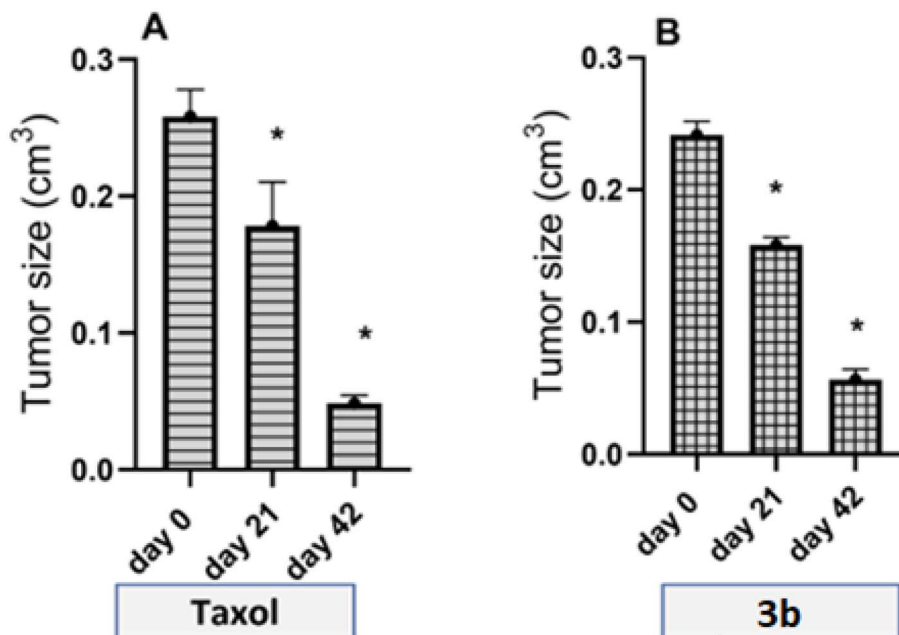The titled compound was separated as green powder with: yield%: 73%, melting point: 218–

Fig. 8 Rats tumour size. Tumour size in diseased rats after treatment at day 0, day 21 and day 42 with the (A) Taxol and (B) synthetic drug **3b**. Data are presented as mean $\pm$ SEM ($n = 6$). Statistical analysis was carried out using one-way ANOVA followed by Tukey's multiple comparison test at p-value < 0.05.

220 °C. FT-IR (ν_{max}, cm^{-1}): 3550–3000 broad band of (O–H), 3010 (Ar C–H), 1680 (alkenic C=C–) and 1650 (C=O of amide). Ms: $m/z\%$: 528.25 [M+] (33.5%). ^{1}H-NMR (400 MHz, DMSO-d$_6$): δ 9.61 (s, 2H, OH, D$_2$O exchangeable), 7.56 (s, 1H, CH=C), 7.07 (dd, $J = 8$, 7.9 Hz, 2H, ArH), 7.08 (dd, $J = 7.5$, 7.9 Hz, 2H, ArH), 7.01 (t, $J = 8.7$ Hz, 2H, ArH), 6.99 (t, $J = 8.2$ Hz, 1H, ArH), 6.98 (dd, $J = 8.1$, 7.6 Hz, 2H, ArH), 6.96 (s, 2H, ArH), 6.86 (d, $J = 8.1$ Hz, 1H, C3–H), 4.75 (s, 2H, CH$_2$–N), 4.74 (d, $J = 8.5$ Hz, 2H, CH$_2$–N), 4.06 (s, 4H, CH$_2$–CH$_3$) 4.05 (q, $J = 8$ Hz, 1H, C3a–H), 1.87 (s, 3H, CH$_3$), 1.31 (t, $J = 7.5$ Hz, 6H, CH$_3$–CH$_2$).

^{13}C-NMR (300 MHz, DMSO-d$_6$): δ 186.11 (C=O), 169.13 (C=N), 136.94, 130.30, 130.15 (ArC), 126.21(C=C), 124.93 (C=C), 116.66, 116.56 (ArC), 116.35 (C=C), 64.41 (1C, C3), 64.35 (CH$_2$–CH$_3$), 47.51 (1C, C3a), 42.86 (CH$_2$–N–CH$_2$), 21.31 (CH$_3$), 15.15

(CH$_3$–CH$_2$). Anal. calcd. for C$_{31}$H$_{33}$N$_3$O$_5$ (527.62):C, 70.57; H, 6.30; N, 7.96, found: C, 70.50; H, 6.33; N, 7.99.

2.5. Biological evaluation

2.5.1. Cytotoxic *in vitro* studies against cell lines. The newly synthesized compounds (**3a–d**), (**4a, b**) & (**5a, b**) were screened for their anti-tumor properties against; human hepatoma (Huh-7), lung cell cancer adenocarcinoma (A549), Michigan Cancer Foundation-7 breast cancer (MCF-7), and for toxicity against Madin–Darby Canine Kidney cells (MDCK cell line) as a model of normal cell line, employing Taxol as standard drug positive reference and utilizing the MTT (3-[4, 5-dimethylthiazol-2-yl]-2, 5 diphenyl tetrazolium bromide) assays reported previously. Four different concentrations of each compound 0.1, 1, 10 and
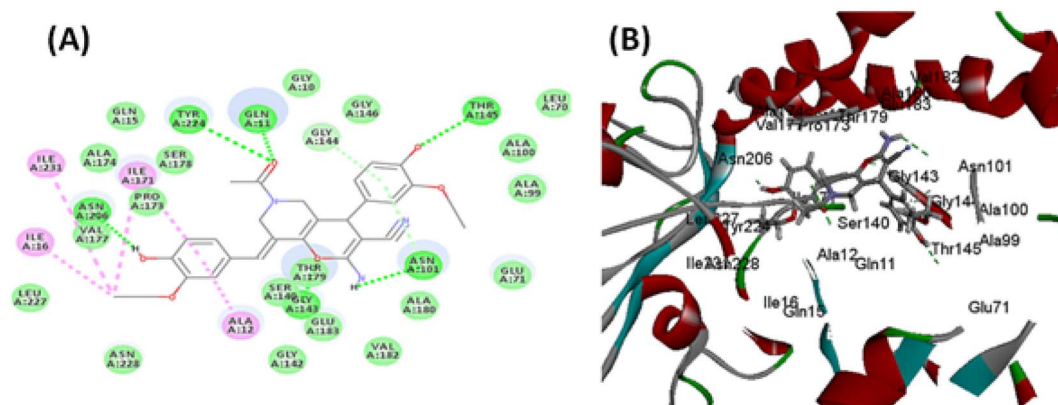

Fig. 9 (A) 2D binding mode of compound **3b**, (B) 3D binding mode of compound **3b** inside tubulin active pocket. Green dotted lines; H-bond, light green dotted lines; van der Waals interactions, purple dotted lines; Pi-alkyl bonds.
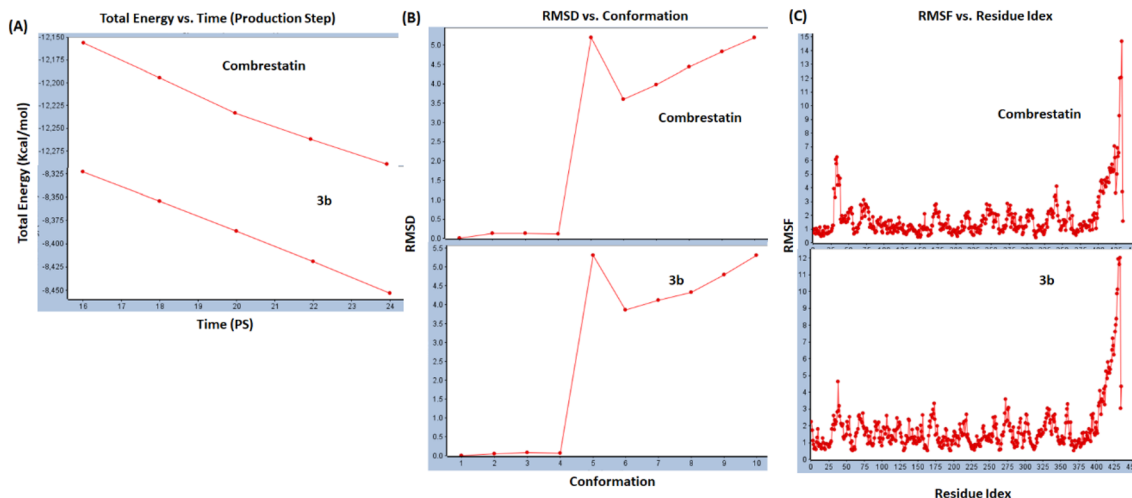
Fig. 10 Dynamic simulation graph plots for **3b** compared to combrestatin: (A); total energy *vs.* time, (B); RMSD *vs.* conformations, (C); RMSF *vs.* residue index.
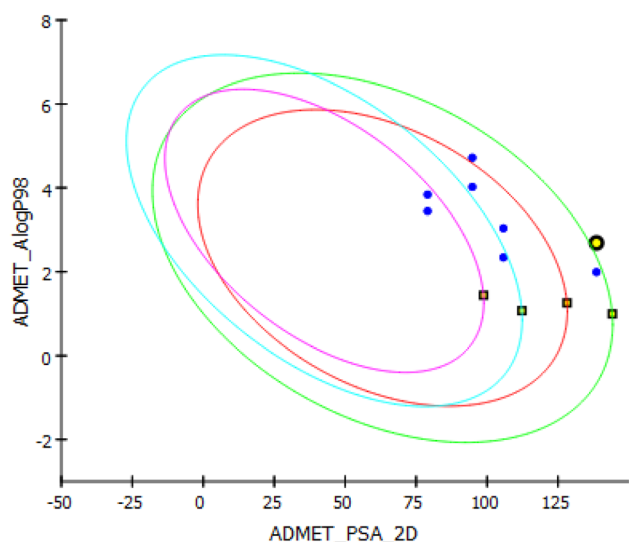

Fig. 11 Graph plot of AMDET study results for all compounds. **3b** is highlighted in yellow.

the untreated control (half maximal inhibitory concentration, IC_{50}) was calculated. For nondividing (primary) cells, drug sensitivity is evaluated as increased cell kill of processed cells in comparison with the loss of cells already usually seen in untreated cells (50% lethal concentration, LC_{50}).[29,30]

2.5.2. Tubulin polymerization assay method. Tubulin fluorescence assay was carried out where, the most active compounds from the *in vitro* cell lines assay were selected (**3a**, **3b**, **5a** and **5b**) and combrestatin (**CA-4**) was utilized as a reference drug. The starting material was 2 mM solution of each compound in DMSO which were then diluted with water to get different concentrations 0.1, 1, 10 and 100 μM for each compound.

The assay volume was 100 μl and the spectrophotometer pathlength was 0.5 cm. The tubulin concentration was 4 mg ml^{-1}. The spectrophotometer was set in kinetic absorbance mode at 340 nm wavelength. The spectrophotometer was set at 37 °C as polymerization reaction was started by the increase in temperature from 4 °C to 37 °C upon transfer of the reaction to a pre-warmed plate.[31]

2.5.3. *In vivo* biological evaluation

2.5.3.1. Animals and experimental design. Eighteen Wistar rats (180–200 g) were obtained from the National Research Centre (Cairo, Egypt). Then rats were housed under normal laboratory conditions (22 ± 2 °C; 12 h/12 h light/dark cycle with

100 μM were prepared to obtain a dose–response curve interpreted as % of cell viability on *y*-axis *versus* concentration in μM on *x*-axis. The drug sensitivity or the concentration needed to reach 50% growth inhibition in comparison with the growth of

Table 3 Results of ADME studies among all compounds

Compound	ADMET solubility level	Absorption level	ADMET BBB level	Hepatotoxicity	PPB
3a	3	1	4	FALSE	FALSE
3b	2	2	4	FALSE	TRUE
3c	2	0	2	TRUE	TRUE
3d	2	0	2	FALSE	TRUE
4a	3	0	3	FALSE	FALSE
4b	2	0	4	FALSE	TRUE
5a	2	0	4	FALSE	TRUE
5b	2	1	4	FALSE	TRUE

Table 4　Results of toxicity studies among all compounds

Compound	TOPKAT Ames applicability	TOPKAT Ames prediction	TOPKAT Ames score	TOPKAT Ames probability	TOPKAT skin irritancy	TOPKAT rat oral LD_{50} g per kg body weight	TOPKAT Rat max. tolerated dose feed g per kg body weight	TOPKAT carcinogenic potency TD_{50} mouse g per kg body weight per day	TOPKAT carcinogenic potency TD_{50} Rat g per kg body weight per day
3a	All properties and	Non-mutagen	−18.63	0.071	Non-irritant	0.19	0.07	53.09	3.29
3b	OPS components		−19.73	0.052		0.40	0.11	36.50	22.30
3c	are within expected		−15.80	0.141		0.05	0.03	6.52	1.26
3d	ranges		−14.25	0.196		0.19	0.02	25.70	45.55
4a			−15.50	0.151		0.25	0.09	75.43	3.20
4b			−16.68	0.115		0.52	0.15	51.90	21.70
5a			−12.45	0.270		0.41	0.11	44.64	5.55
5b			−13.59	0.222		0.86	0.18	30.60	37.53

free access to food and water). Mammary tumors were induced as previously described. Once the tumors volume reached 1 cm³, the rats were divided randomly into 2 different groups as follows:

● Group 1: untreated control group (C) $n = 6$.

● Group 2: breast induced cancer group (BC) $n = 12$.

To induce breast cancer, 7,12-dimethylbenz[*a*]anthracene (DMBA) supplied by Sigma-Aldrich company (St. Louis, MO, USA) was used. Rats in (Group 2) were injected intraperitoneally each with a single dose of 20 mg kg⁻¹ body weight of DMBA dissolved in corn oil and given in a volume of 0.5 ml.[32,33]

Rats were palpated weekly to check for tumor appearance; the first detection of tumor was after three months (90 days). After 120 days, (Group 2) was divided into 2 subgroups, one was treated with Taxol and the other was treated with the synthetic drug (**3b**) at the same dose.

At the end of treatment period, rats from all groups were killed using a lethal dose of thiopental (IP 200 mg kg⁻¹).

2.5.3.2.　Histopathology. Samples from autopsy were taken from breast tissues of rats in different groups and fixed in 10% formal saline for twenty-four hours. Washing was done using tap water then serial dilutions of ethyl alcohol were used for dehydration. Specimens were cleared in xylene and embedded in paraffin at 56° in hot air oven for twenty-four hours. Paraffin bees wax tissue blocks were prepared for sectioning at 4 μm thickness by sledge microtome. The obtained tissue sections were collected on glass slides, deparaffinized, stained by hematoxylin and eosin (H&E) stain for examination through light electric microscope.[34]

2.5.3.3.　Tumor volume and body weight. Tumor volume and body weight was recorded 3 times throughout the treatment, once after the end of the induction (day 0), once at 3 weeks of treatment (day 21) and at the end of treatment after 6 weeks of treatment (day 42). Animal handling followed the Guide for the Care and Use of Laboratory Animals.[35] The experiments were approved by the ethics committee in the Future University in Egypt (REC-FPSPI-14/110).

2.6.　Computational studies

In search for the mechanism of inhibition behavior presented by the newly synthesized compounds for tubulin in the *in vitro* assays, molecular docking studies were performed on tubulin-podophyllotoxin: stathmin-like domain complex using Discovery Studio 4.1. Using the same software, dynamic simulation studies were also performed to check the stability of this interaction inhibition. Moreover, to validate the pharmacokinetic properties from the points of absorption, distribution, metabolism, and excretion ADME studies were performed side by side to *in silico* toxicity studies to inform the safety of the new structural compounds.

2.6.1.　Molecular docking. The tubulin protein was downloaded from protein data bank with code: 1SA1. The protein was prepared, and missing residues were supplied. Hydrogen atoms were later added, and energy simulation was applied using CHARMM forcefield and MMFF as partial charge. A heavy atom of the protein was then built up and the whole atom constraints were fixed to allow flexibility of ligands only. Energy minimization was applied, the receptor of the output molecule was identified, and the active sites were determined as downloaded from protein data bank.[36] Similarly, to the *in vitro* studies **CA-4** was used as a reference ligand and its structure was downloaded from PUBCHEM as ".sd format". The new molecules; **3a–d, 4a, 4b, 5a** and **5b** were drawn and checked on Chemdraw and saved as ".mol format" file to be readable on Discovery Studio. Both reference and the new compounds were subjected to same forcefield of protein as simulation; CHARMM and MMFF and prepared as ligands using software protocols. The output molecules were allowed to dock within the prepared protein *via* C-docker protocol to give 10 conformations for each compound with various – (c-docker interaction energies). The visualization of both 2D and 3D modes of interactions were applied also using Discovery Studio.

2.6.2.　Dynamic simulations. The dynamic simulation studies were carried out using Discovery Studio 4.1 and applied to **CA-4** & **3b** against tubulin. Standard Dynamic Cascades protocol was applied, and minimization algorithm used was (steepest descent) with maximum 2000 steps. RMS gradient was set to be 1.0 and the second minimization algorithm used was (conjugate gradient) with maximum 1000 steps. Initial temperature was adjusted to be 50 °C and target temp. 300 °C with maximum velocity 2000. Simulation time of Equilibration phase was set 10 Ps and interval 2 Ps. The Implicit Solvent

Model used was Generalized Born with Simple Switching (GBSW) and LeapfroyVerlet protocol was used as the dynamic's integrator.[36]

2.6.3. ADME & TOPKAT toxicity studies. ADMET protocol was applied to prepared ligands of both **CA-4** and the new compounds. Graph plot and numerical schedules were produced and presented.[37]

Similarly, TOPKAT toxicity protocol was applied to previously prepared ligands after selection of criteria to be measured; Ames applicability, prediction, score, probability, skin irritancy, rat oral LD_{50}, Rat Max. Tolerated Dose Feed Carcinogenic Potency TD_{50} for both mouse and rat.

3. Results and discussion

3.1. Rational & chemistry

Literature studies exposed the structural activity relationship carried out on curcumin piperidone analogues which revealed that the 1,5-diaryl-3-oxo-1,4-pentadienyl pharmacophore is very essential in activity of the compound as this group reacts with cellular components at a specific binding site (primary binding site)[38] (Fig. 3). Alignment of the 1,5-diaryl-3-oxo-1,4-pentadienyl group at the primary site may be affected by the nature of the group attached to the heterocyclic nitrogen atom.[39–41] This group increased the cytotoxic potencies due to either extra binding with cellular constituents at the auxiliary binding site or by easing the interaction of the cytotoxin at the primary site.[42] On the contrary, the group attached on the nitrogen atom may result in potency reduction because of the repulsion between this bulky group and the auxiliary site therefore, preventing interaction between the 1,5-diaryl-3-oxo-1,4-pentadienyl moiety and the primary binding site.[43] Hence, bulky groups were avoided in the novel compounds and acetyl group was added on nitrogen instead.[44]

It was also discovered that the charged molecules may be incapable of penetrating cell membranes and making a cytotoxic effect. Therefore, *N*-acylation was deemed a route to pursue making nitrogen atom in a non-basic form. An oxygen atom of the acyl group linked to the heterocyclic nitrogen atom may enable hydrogen bonding with the auxiliary site.[45–48]

The synthesis of the target compounds followed the pathway outlined in Scheme 1. The intermediate compounds **2a–d** were prepared in one step. Briefly, aldol condensation of the appropriate aldehydes was carried out with *N*-acetyl-4-piperidone. Subsequently, the target compounds **3a–d**, **4a**, **4b**, **5a** and **5b** were produced *via* cyclization of intermediate compounds using either malononitrile for series 3, thiourea for series 4 or phenylhydrazine for series 5. The chemical structures of newly synthesized compounds were confirmed and characterized *via* performing various elemental and spectral data.

3.2. Biological evaluation

3.2.1. *In vitro* **antiproliferative activities and cytotoxicity assay.** All the newly synthesized pyridine heterocyclic hybrids were examined against three types of cancer cell lines; hepatocyte derived carcinoma, lung cancer and breast cancer; (Huh-7, (A549) and (MCF-7) respectively. Cells were treated with different concentrations of each compound, and the cell viability was measured using MTT assay employing Taxol as the positive reference standard drug (Table 1). Taxol displayed IC_{50} = 6.68, 38.05, and 12.32 μM against Huh-7, A549 and MCF-7, respectively. On the other hand, the new compounds showed moderate to extremely potent activity against the three cell lines except for compound **3d**. Series 3 & series 5 compounds displayed activity on the three cell lines better than series 4 which suggested that pyrano-pyridine and pyrazolo-pyridine hybrids are more promising. Additionally, methoxy/ethoxy diarylidene derivatives presented enhanced activity than *p*-chlorphenyl/cinnmaldehyde derivatives. Compound **3b** displayed superior activity with IC_{50} = 6.54, 15.54, 6.13 μM against Huh-7, A549 and MCF-7, respectively.

According to the above analysis, some structure–activity relationship (SAR) could be concluded: the introduction of fused-heterocyclic moiety was found effective and almost all the tested compounds showed moderate to potent antiproliferative activity. Also, it could be observed that methoxy and ethoxy groups attached to phenyl ring were an essential pharmacophore for retaining bioactivities, which is consistent with previously reported compounds.[9,13]

3.2.2. Cytotoxicity test against normal cells. Cytotoxic effect of the most potent compounds; **3a**, **3b**, **5a** and **5b** was tested against Madin–Darby Canine Kidney cells (MDCK) as noncancerous cells, and Taxol was used as positive control. As shown in (Fig. 4), the data showed that the cytotoxicity of all the tested compounds was obviously less than Taxol. Taxol displayed IC_{50} value of 0.85 μM against MDCK normal cells. While compounds **3a**, **3b**, **5a** and **5b** possessed IC_{50} values of 3.97, 8.11, 6.53, and 6.02 μM respectively. The least toxic compound was **3b**.

3.2.3. Morphological assessment. Because of the importance of microtubules in the maintenance of cell morphology, morphological assessment test was performed to reveal whether compound **3b** could affect microtubule morphology in living cells. Cell morphology has been detected in comparison to untreated control, and positive control treated with Taxol using inverted light microscope. The morphological assessment for the (A549) cells treated with the 100 μM of compound **3b** or Taxol for 48 h, compared to untreated control showed apparent cell toxicity which was evident by loss of monolayer sheet (Red arrow), increasing in cell lysis, and shrinkage of cells (Blue arrow) as shown in (Fig. 5). The effect of compound **3b** was comparable to the effect of the reference drug Taxol at this concentration. These results were in a good agreement with MTT assay results, which depicted potential cytotoxic effect of compound **3b** on (A549) cells.[49]

3.2.4. Tubulin polymerisation assay. Highly dynamic mitotic-spindle microtubules are amongst the most efficient targets for anticancer therapy There are three diverse target sites on the tubulin heterodimer, namely the colchicine, the vinca alkaloids and paclitaxel binding sites. However, **CA-4** is a class of vascular disrupting agents that target existing tumor blood through acting on β-subunit of tubulin at what is called the colchicine site, and cause depolymerization of tubulin.

To investigate whether the antiproliferative activities of compounds; **3a**, **3b**, **5a** and **5b** is linked to the mechanism of tubulin depolymerization, these agents were evaluated for their inhibition of tubulin polymerization in comparison to **CA-4** as a reference depolymerizing agent.

The assay yielded results displayed in Table 2. All compounds showed good ability to inhibit tubulin polymerisation with IC_{50} values ranging from 4.03 to 15.60 μg ml^{-1} and inhibition % ranging from 69% to 81%. Compound **3b** had the most inhibitory effect with IC_{50} of 4.03 μg ml^{-1} and 81% inhibition which is comparable to the reference drug **CA-4** that displayed inhibition of 86% and $IC_{50} = 1.64$ μg ml^{-1}.

3.2.5. In vivo biological evaluation. The antitumor effects of compound **3b** were evaluated in vivo. Mammary tumours were induced in 18 female Wistar rats. The rats were divided into 2 groups, group 1 as a (control untreated group) and group 2 as (breast cancer induced group). The first detection of tumour was after three months (90 days) of induction. After 120 days, group 2 was divided into 2 subgroups, one was treated with Taxol and the other was treated with the synthetic drug **3b** at a dose of 2 mg per kg per week.[50,51] Values were presented as mean ± SEM of 6 animals. Significant difference between groups was carried out using analysis of variance (ANOVA) followed by Tukey's post hoc test. Significance was taken as $P < 0.05$.

Microscopic examination of the control group (C) using hematoxylin and eosin (H&E) stain showed normal histology structure of mammary gland lobules which consisted of tubule-alveolar glands that were formed of branched system of ducts and secretory alveoli arranged in multiple lobules. Examination of covering skin showed normal epidermis and dermis with intact subcutaneous connective tissue (Fig. 6). The breast cancer group (BC) showed necrosis of the epithelial covering mammary gland. The mammary epithelia showed dysplastic changes that revealed numerous proliferating neoplastic cells that invaded surrounding tissues. The tumor cells showed hyperchromatic nuclei with few prominent nucleoli which were arranged in multilayer structure that narrowed the ductal lumen.

Histopathology results showed that the intensity of inflammatory cells infiltrates decreased after treatment with both Taxol and **3b** (synthetic drug) as shown in (Fig. 7).

Mammary adenocarcinoma was observed in some examined sections and was characterized by solid aggregations of neoplastic cells associated with numerous mononuclear inflammatory cells infiltration[34] (Fig. 7).

Tumor size and body weight of Wistar rats were measured and recorded 3 times throughout the treatment, once after the end of the induction (day 0), once at 3 weeks of treatment (day 21) and once at the end of treatment/after 6 weeks of treatment (day 42) to determine whether drug **3b** could target breast cancer cell growth. Both Taxol and **3b** did not have a significant effect on rats' body weights.

On the other hand, for the antitumor study, tumor size of the **3b**-treated rats was significantly decreased by 79% at the end of the treatment compared to the tumor size before initiation of the treatment at $P < 0.05$ as shown in (Fig. 8) which was comparable to that of Taxol which showed 81% inhibition.

3.3. In silico studies

3.3.1. Molecular modeling studies. Based on the previously obtained in vitro assay results of the tubulin inhibition assay, it was essential to figure out the mechanism of binding of compounds with tubulin. Tubulin was downloaded with PDB code: 1SA1 (ref. 52) and prepared as previously discussed in methodology. The prepared compounds were allowed to dock into the active pocket of protein using C-docker protocol. The obtained – (c-docker interaction energies) were sorted for each 10 obtained compound conformations and only least energy with best conformer were presented in (Table S21 in ESI†) together with its 2D binding mode. The results of our compounds were compared to reference selected drug **CA-4**. **CA-4** displayed interaction with main key amino acids; Gln 11, Ala 12 and the most important Thr 145 via H-bond, π-bond, and H-bond respectively. The c-docker interaction energy of **CA-4** was −38.52 kcal mol^{-1}, while the new compounds were in the range of (−45.44–54.83) kcal mol^{-1}. Compounds **3a** and **3b** displayed same binding with key amino acids as reference compound with extra favorable interactions and better energy for compound **3b** as shown in (Fig. 9). Compounds **3c**, **3d**, **4a** and **4b** missed the essential H-bond with Thr 145. While compounds **5a** and **5b** failed in the interaction with chain A but displayed different mechanism through chain B interaction. These findings coincide with the in vitro protein inhibition assay where compounds **3a** and **3b** showed superior tubulin inhibition over **5a** and **5b** owing to the pyrano-pyridine ring size that formed correct orientation of the essential functional groups into the active binding site.

3.3.2. Standard dynamic simulations. To re-ensure the stability of ligands binding to protein and production of effective inhibition, molecular dynamic simulation studies are applied. The best active conformer of the reference **CA-4** obtained from the docking study was selected for its dynamic stability inside tubulin active site and compared to that of the best active compound **3b**. Results obtained in (Fig. 10) represented total energy produced during the production phase over time, root mean square deviations (RMSD) and root mean square fluctuations (RMSF) for ten best produced conformations of both **CA-4** and **3b** in the docked poses. The total energy produced by **CA-4** was (12 150–12 275) kcal mol^{-1} over time range (16–24) ps and 9 new hydrogen bonds were formed between **CA-4** and tubulin. While over similar timeline **3b** produced comparable stable total energy (8325–8450) kcal mol^{-1} and 8 new hydrogen bonds were formed between **3b** and tubulin. The total energy decreases overtime which indicated interaction stability. On the other hand, RMSD showed that the deviations of both **CA-4** and **3b** were similar within the accepted. Steady fluctuations for both **CA-4** and **3b** were similar and within accepted ranges, where most fluctuations were below 3.5.

3.3.3. ADME studies. To get more in depth into the pharmacokinetic properties of the designed compounds, ADMET

studies were performed using Discovery Studio 4.1. Intestinal absorption, solubility, hepatotoxicity, ability to pass blood–brain barrier (BBB) and ability to bind to plasma protein (PPB) were all measured for all compounds (Fig. 11). Results were tabulated in (Table 3) and as shown the solubility levels (2) for most compounds stated that they were low soluble except compounds **3a** and **4a** were found to be at level (3) meaning they possessed good solubility. Intestinal absorption of compounds was between good to moderate absorption. The ability to pass BBB was at level 4 which reflected very low ability and hence less expected side effects. All compounds were not hepatotoxic except the probability of compound **3c**. Most compounds have the ability to bind to plasma protein which indicated their prolonged duration of action except for compounds **3a** and **4a**.

    3.3.4. Toxicity studies. TOPKAT Ames Toxicity protocol was adopted to evaluate possible toxicities to all new compounds. All TOPKAT Ames probabilities, applications & scores showed that compounds are non-mutagenic, non-carcinogenic nor irritant and were all within expected ranges (Table 4).

4. Conclusion

A series of novel pyridine heterocyclic hybrids were designed, synthesized, and evaluated for their *in vitro* anticancer activity against human hepatoma (Huh-7), lung cell cancer adenocarcinoma (A549), and breast cancer (MCF-7). Most of the novel pyridine hybrids exhibited potent cytotoxicity. Moreover, tubulin inhibitory effect of the most potent compounds was assessed, and they showed good tubulin inhibition activity. Compound **3b** was found to be the most potent compound possessing cytotoxic activity on cancer cell lines with $IC_{50} = 6.54$ μM against (Huh-7) liver cancer cell line and $IC_{50} = 6.13$ μM against (MCF-7) breast cancer cell line. Also, compound **3b** showed great ability to inhibit tubulin polymerization with superior value of IC50 = 4.03 μM (81% inhibition) compared to **CA-4** the reference drug. These results also coincide with the docking interaction energy score (-48.22 kcal mol^{-1}) which was obtained from the *in silico* study. Compound **3b** was also the least toxic compound against the non-cancerous cells with IC_{50} of 8.11 μM. Also, compound **3b** was able to suppress tumour size in experimental rats by 79% according to (*in vivo* studies). These findings have proven that pyrano-pyridine ring could be an essential feature for further new anticancer scaffolds.

Ethical statement

The experiments were approved by the ethics committee in the Future University in Egypt (REC-FPSPI-14/110).

Author contributions

Menna M. Abdelshaheed: contributed to the synthesis of the compounds, collecting literature studies and data, interpretation of the results and writing the scientific article. Hussein I. El Subbagh: contributed to the idea of work, scheme suggestion, writing and revision of the scientific article. Mohamed A. Tantawy: contributed to the *in vitro* biological assays and writing the results. Reem T. Attia: contributed to the *in vivo* biological assays and writing the results. Khairia M. Youssef: contributed to the idea of work, scheme suggestion, writing and revision of the scientific article. Iten M. Fawzy: contributed to the idea of work, scheme suggestion, molecular modeling, dynamic studies, toxicity and ADME studies, writing and revision of the scientific article.

Conflicts of interest

We declare that the authors have no competing interests.

References

1 H. Q. Daniel, P. Mathurin, H. Cortez-Pinto and R. Loomba, Global epidemiology of alcohol-associated cirrhosis and HCC: trends, projections and risk factors, *Nat. Rev. Gastroenterol. Hepatol.*, 2023, **20**(1), 37–49, DOI: 10.1038/s41575-022-00688-6.

2 K. Peter, A. Ahmed and D. Kim, Causes and risk profiles of mortality among individuals with nonalcoholic fatty liver disease, *Clin. Mol. Hepatol.*, 2023, **29**, S43, DOI: 10.3350/cmh.2022.0351.

3 M. Berkman Amy, N. Mittal and M. E. Roth, Adolescent and young adult cancers: unmet needs and closing the gaps, *Curr. Opin. Pediatr.*, 2023, **35**(1), 84–90, DOI: 10.1097/MOP.0000000000001200.

4 R. Sahu, R. Mishra, R. Kumar, C. Majee, A. Mazumder and A. Kumar, Pyridine moiety: an insight into recent advances in the treatment of cancer, *Mini-Rev. Med. Chem.*, 2022, **22**(2), 248–272, DOI: 10.2174/1389557521666210614162031.

5 Y. Ling, Z. Y. Hao, D. Liang, C. L. Zhang, Y. F. Liu and Y. Wang, The expanding role of pyridine and dihydropyridine scaffolds in drug design, *Drug Des., Dev. Ther.*, 2021, **15**, 4289–4338, DOI: 10.2147/DDDT.S329547.

6 G. Bérubé, An overview of molecular hybrids in drug discovery, *Expert Opin. Drug Discovery*, 2016, **11**(3), 281–305, DOI: 10.1517/17460441.2016.1135125.

7 Y. Lu, J. Chen, M. Xiao, W. Li and D. D. Miller, An overview of tubulin inhibitors that interact with the colchicine binding site, *Pharm. Res.*, 2020, **29**, 2943–2971, DOI: 10.1007/s11095-012-0828-z.

8 G. Ş. Karatoprak, E. Küpeli Akkol, Y. Genç, H. Bardakcı, Ç. Yücel and E. Sobarzo-Sánchez, Combretastatins: an overview of structure, probable mechanisms of action and potential applications, *Mol*, 2020, **25**(11), 2560, DOI: 10.3390/molecules25112560.

9 I. M. Fawzy, K. M. Youssef, N. S. Ismail, J. Gullbo and K. A. Abouzid, Newly designed and synthesized curcumin analogs with in vitro cytotoxicity and tubulin polymerization activity, *Chem. Biol. Drug Des.*, 2015, **86**(1), 80–90, DOI: 10.1111/cbdd.12464.

10 M. Mahdavi, S. Asghari, M. Rahnamay, G. Dehghan, M. A. H. Feizi and S. Balalaie, Cytotoxicity, oxidative stress, and apoptosis in K562 leukemia cells induced by an active compound from pyrano-pyridine derivatives, *Hum. Exp.*

Toxicol., 2018, **37**(10), 1105–1116, DOI: **10.1177/ 0960327118756719**.

11 K. M. Youssef, M. A. Al-Omar, H. I. El-Subbagh, L. A. Abou-Zeid, A. G. M. Abdel-Gader, N. G. Haress and A. S. Al-Tuwaijri, Synthesis, antiplatelet aggregation activity, and molecular modeling study of novel substituted-piperazine analogues, *Med. Chem. Res.*, 2011, **20**, 898–911, DOI: **10.1007/s00044-010-9411-5**.

12 I. W. Cheney, S. Yan, T. Appleby, H. Walker, T. Vo, N. Yao, R. Hamatake, Z. Hong and J. Z. Wu, Identification and structure–activity relationships of substituted pyridones as inhibitors of Pim-1 kinase, *Bioorg. Med. Chem. Lett.*, 2007, **17**(6), 1679–1683, DOI: **10.1016/j.bmcl.2006.12.086**.

13 H. I. El-Subbagh, S. M. Abu-Zaid, M. A. Mahran, F. A. Badria and A. M. Al-Obaid, Synthesis and biological evaluation of certain α, β-unsaturated ketones and their corresponding fused pyridines as antiviral and cytotoxic agents, *J. Med. Chem.*, 2000, **43**(15), 2915–2921, DOI: **10.1021/jm000038m.**

14 A. Farce, C. Loge, S. Gallet, N. Lebegue, P. Carato, P. Chavatte, P. Berthelot and D. Lesieur, Docking study of ligands into the colchicine binding site of tubulin, *J. Enzyme Inhib. Med. Chem.*, 2004, **19**(6), 541–547, DOI: **10.1080/14756360412331280545**.

15 N. Mizuno, S. Toba, M. Edamatsu, J. Watai-Nishii, N. Hirokawa, Y. Y. Toyoshima and M. Kikkawa, Dynein and kinesin share an overlapping microtubule-binding site, *EMBO J.*, 2004, **23**(13), 2459–2467, DOI: **10.1038/ sj.emboj.7600240**.

16 D. E. Pryor, A. O'Brate, G. Bilcer, J. F. Díaz, Y. Wang, M. Kabaki, M. K. Jung, J. M. Andreu, A. K. Ghosh and P. Giannakakou, The microtubule stabilizing agent laulimalide does not bind in the taxoid site, kills cells resistant to paclitaxel and epothilones, and may not require its epoxide moiety for activity, *Biochemistry*, 2002, **41**(29), 9109–9115, DOI: **10.1021/bi020211b**.

17 Y. T. Wang, T. Q. Shi, H. L. Zhu and C. H. Liu, Synthesis, biological evaluation and molecular docking of benzimidazole grafted benzsulfamide-containing pyrazole ring derivatives as novel tubulin polymerization inhibitors, *Bioorg. Med. Chem.*, 2019, **27**(3), 502–515, DOI: **10.1016/ j.bmc.2018.12.031**.

18 R. Gaspari, A. E. Prota, K. Bargsten, A. Cavalli and M. O. Steinmetz, Structural basis of cis-and trans-combretastatin binding to tubulin, *Chem*, 2017, **2**(1), 102–113, DOI: **10.1016/j.chempr.2016.12.005**.

19 A. S. Negi, Y. Gautam, S. Alam, D. Chanda, S. Luqman, J. Sarkar, F. Khan and R. Konwar, Natural antitubulin agents: Importance of 3, 4, 5-trimethoxyphenyl fragment, *Bioorg. Med. Chem.*, 2015, **23**(3), 373–389, DOI: **10.1016/ j.bmc.2014.12.027**.

20 W. Li, H. Sun, S. Xu, Z. Zhu and J. Xu, Tubulin inhibitors targeting the colchicine binding site: a perspective of privileged structures, *Future Med. Chem.*, 2017, **9**(15), 1765–1794, DOI: **10.4155/fmc-2017-0100**.

21 K. Prasat, Anticancer drugs and potential anticancer leads inspired by natural products, *Stud. Nat. Prod. Chem.*, 2015, **44**, 251–307, DOI: **10.1016/B978-0-444-63460-3.00005-5**.

22 B. Onel, M. Carver, G. Wu, D. Timonina, S. Kalarn, M. Larriva and D. Yang, A new G-quadruplex with hairpin loop immediately upstream of the human BCL2 P1 promoter modulates transcription, *J. Am. Chem. Soc.*, 2016, **138**(8), 2563–2570, DOI: **10.1021/jacs.5b08596**.

23 C. D. Churchill, M. Klobukowski and J. A. Tuszynski, The unique binding mode of laulimalide to two tubulin protofilaments, *Chem. Biol. Drug Des.*, 2015, **86**(2), 190–199, DOI: **10.1111/cbdd.12475**.

24 M. A. Jordan and L. Wilson, Microtubules as a target for anticancer drugs, *Nat. Rev. Cancer*, 2004, **4**(4), 253–265, DOI: **10.1038/nrc1317**.

25 I. Mamdouh, K. Youssef, N. Ismail, J. Gullbo and K. Abouzid, Design and Synthesis and Biological evaluation of Novel Curcumin Analogs with anticipated anticancer activity, *Future J. Pharm. Sci.*, 2015, **1**, 22, DOI: **10.1016/ j.fjps.2015.06.001**.

26 U. Das, J. Alcorn, A. Shrivastav, R. K. Sharma, E. De Clercq, J. Balzarini and J. R. Dimmock, Design, synthesis and cytotoxic properties of novel 1-[4-(2-alkylaminoethoxy) phenylcarbonyl]-3, 5-bis (arylidene)-4-piperidones and related compounds, *Eur. J. Med. Chem.*, 2007, **42**(1), 71–80, DOI: **10.1016/j.ejmech.2006.08.002**.

27 H. A. Soliman, M. N. M. Yousif, M. M. Said, N. A. Hassan, M. M. Ali, H. M. Awad and F. M. Abdel-Megeid, Synthesis of novel 1, 6-naphthyridines, pyrano [3, 2-c] pyridines and pyrido [4, 3-d] pyrimidines derived from 2, 2, 6, 6-tetramethylpiperidin-4-one for in vitro anticancer and antioxidant evaluation, *Der Pharma Chem.*, 2014, **6**(3), 394–410.

28 M. S. Nafie, A. M. Amer, A. K. Mohamed and E. S. Tantawy, Discovery of novel pyrazolo[3,4-b]pyridine scaffold-based derivatives as potential PIM-1 kinase inhibitors in breast cancer MCF-7 cells, *Bioorg. Med. Chem.*, 2020, **28**(24), 115828, DOI: **10.1016/j.bmc.2020.115828**.

29 J. van Meerloo, G. J. Kaspers and J. Cloos, Cell sensitivity assays: the MTT assay, *Methods Mol. Biol.*, 2011, **731**, 237–245, DOI: **10.1007/978-1-61779-080-5_20**.

30 H. Ali-Boucetta, K. T. Al-Jamal and K. Kostarelos, Cytotoxic assessment of carbon nanotube interaction with cell cultures, *Methods Mol. Biol.*, 2011, **726**, 299–312, DOI: **10.1007/978-1-61779-052-2_19**.

31 T. Zhu, S. H. Wang, D. Li, S. Y. Wang, X. Liu, J. Song, Y. T. Wang and S. Y. Zhang, Progress of tubulin polymerization activity detection methods, *Bioorg. Med. Chem. Lett.*, 2021, **37**, 127698, DOI: **10.1016/ j.bmcl.2020.127698**.

32 N. El-Azem, M. Pulido-Moran, C. L. Ramirez-Tortosa, J. L. Quiles, F. E. Cara, P. Sanchez-Rovira, S. Granados-Principal and M. Ramirez-Tortosa, Modulation by hydroxytyrosol of oxidative stress and antitumor activities of paclitaxel in breast cancer, *Eur. J. Nutr.*, 2019, **58**(3), 1203–1211, DOI: **10.1007/s00394-018-1638-9**.

33 K. Batcioglu, A. B. Uyumlu, B. Satilmis, B. Yildirim, N. Yucel, H. Demirtas, R. Onkal, R. M. Guzel and M. B. Djamgoz, Oxidative Stress in the in vivo DMBA Rat Model of Breast Cancer: Suppression by a Voltage-gated Sodium Channel

Inhibitor (RS 100642), *Basic Clin. Pharmacol. Toxicol.*, 2012, **111**(2), 137–141, DOI: 10.1111/j.1742-7843.2012.00880.x.

34 J. D. Bancroft, A. Stevens, and D. R. Turner, *Theory and Practice of Histological Techniques*, Churchill Livingstone, London, Toronto, 4th edn, 1996.

35 National Research Council (US), *Committee for the Update of the Guide for the Care and Use of Laboratory Animals. Guide for the Care and Use of Laboratory Animals*, Washington (DC), National Academies Press (US), 8th edn, 2011.

36 S. Saxena, M. Abdullah, D. Sriram and L. Guruprasad, Discovery of novel inhibitors of Mycobacterium tuberculosis MurG: Homology modelling, structure based pharmacophore, molecular docking, and molecular dynamics simulations, *J. Biomol. Struct. Dyn.*, 2018, **36**(12), 3184–3198, DOI: 10.1080/07391102.2017.1384398.

37 S. Sahu, S. K. Ghosh, P. Gahtori, U. P. Singh, D. R. Bhattacharyya and H. R. Bhat, In silico ADMET study, docking, synthesis and antimalarial evaluation of thiazole-1, 3, 5-triazine derivatives as Pf-DHFR inhibitor, *Pharmacol. Rep.*, 2019, **71**(5), 762–767, DOI: 10.1016/j.pharep.2019.04.006.

38 U. Das, R. K. Sharma and J. R. Dimmock, 1, 5-diaryl-3-oxo-1, 4-pentadienes: a case for antineoplastics with multiple targets, *Curr. Med. Chem.*, 2009, **16**(16), 2001–2020, DOI: 10.2174/092986709788682218.

39 N. Edraki, U. Das, B. Hemateenejad, J. R. Dimmock and R. Miri, Comparative QSAR Analysis of 3,5-bis (Arylidene)-4-Piperidone Derivatives: The Development of Predictive Cytotoxicity Models, *Iran. J. Pharm. Res.*, 2016, **15**(2), 425–437.

40 V. M. Muzalevskiy, O. V. Serdyuk, and V. G. Nenajdenko, Chemistry of fluorinated indoles, *Fluorine in Heterocyclic Chemistry*, 2014, vol. 1, pp. 117–156.

41 M. Helal, *Investigation of Some Molecular Mechanisms of Cytotoxic 1, 5-diaryl-3-oxo-1, 4-pentadienes*, Doctoral dissertation, University of Saskatchewan, Canada, 2012.

42 K. M. Lakhani, *Synthesis and Bioactivities of Novel N^1-Acylhydrazides*, Doctoral dissertation, University of Saskatchewan, Canada, 2018.

43 Y. Lu, J. Chen, M. Xiao, W. Li and D. D. Miller, An overview of tubulin inhibitors that interact with the colchicine binding site, *Pharm. Res.*, 2012, **29**(11), 2943–2971, DOI: 10.1007/s11095-012-0828-z.

44 J. Sun, S. Zhang, C. Yu, G. Hou, X. Zhang, K. Li and F. Zhao, Design, Synthesis and Bioevaluation of Novel N-Substituted-3, 5-Bis (Arylidene)-4-piperidone Derivatives as Cytotoxic and Antitumor Agents with Fluorescent Properties, *Chem. Biol. Drug Des.*, 2014, **83**(4), 392–400, DOI: 10.1111/cbdd.12254.

45 M. Hossain, C. E. Enci, J. R. Dimmock and U. Das, Discovery and investigation of 1-[4-(2-aminoethoxy) phenylcarbonyl]-3, 5-bis-(benzylidene)-4-piperidones as candidate antineoplastic agents: Our last 15 years study, *Curr. Med. Chem.*, 2021, **28**(13), 2453–2464, DOI: 10.2174/0929867327666200730215752.

46 E. Robles-Escajeda, U. Das, N. M. Ortega, K. Parra, G. Francia, J. R. Dimmock, A. Varela-Ramirez and J. R. Aguilera, A novel curcumin-like dienone induces apoptosis in triple-negative breast cancer cells, *Cell. Oncol.*, 2016, **39**, 265–277, DOI: 10.1007/s13402-016-0272-x.

47 M. Hossain, U. Das, N. Umemura, H. Sakagami, J. Balzarini, E. De Clercq, M. Kawase and J. R. Dimmock, Tumour-specific cytotoxicity and structure–activity relationships of novel 1-[3-(2-methoxyethylthio) propionyl]-3, 5-bis (benzylidene)-4-piperidones, *Bioorg. Med. Chem.*, 2016, **24**(10), 2206–2214, DOI: 10.1016/j.bmc.2016.03.056.

48 M. Nakhjiri, M. Safavi, E. Alipour, S. Emami, A. F. Atash, M. Jafari-Zavareh, S. K. Ardestani, M. Khoshneviszadeh, A. Foroumadi and A. Shafiee, Asymmetrical 2,6-bis(benzylidene)cyclohexanones: Synthesis, cytotoxic activity and QSAR study, *Eur. J. Med. Chem.*, 2012, **50**, 113–123, DOI: 10.1016/j.ejmech.2012.01.045.

49 C. Dyrager, M. Wickström, M. Fridén-Saxin, A. Friberg, K. Dahlén, E. A. Wallén, J. Gullbo, M. Grøtli and K. Luthman, Inhibitors and promoters of tubulin polymerization: Synthesis and biological evaluation of chalcones and related dienones as potential anticancer agents, *Bioorg. Med. Chem.*, 2011, **19**(8), 2659–2665, DOI: 10.1016/j.bmc.2011.03.005.

50 N. El-Azem, M. Pulido-Moran, C. L. Ramirez-Tortosa, J. L. Quiles, F. E. Cara, P. Sanchez-Rovira, S. Granados-Principal and M. Ramirez-Tortosa, Modulation by hydroxytyrosol of oxidative stress and antitumor activities of paclitaxel in breast cancer, *Eur. J. Nutr.*, 2019, **58**, 1203–1211, DOI: 10.1007/s00394-018-1638-9.

51 K. Batcioglu, A. B. Uyumlu, B. Satilmis, B. Yildirim, N. Yucel, H. Demirtas, R. Onkal, R. M. Guzel and M. B. Djamgoz, Oxidative stress in the in vivo DMBA rat model of breast cancer: suppression by a voltage-gated sodium channel inhibitor (RS100642), *Basic Clin. Pharmacol. Toxicol.*, 2012, **111**(2), 137–141, DOI: 10.1111/j.1742-7843.2012.00880.x.

52 R. B. Ravelli, B. Gigant, P. A. Curmi, I. Jourdain, S. Lachkar, A. Sobel and M. Knossow, Insight into tubulin regulation from a complex with colchicine and a stathmin-like domain, *Nature*, 2004, **428**(6979), 198–202, DOI: 10.1038/nature02393.